

Temporal-mode-selective optical Ramsey interferometry via cascaded frequency conversion

Dileep V. Reddy* and Michael G. Raymer

*Oregon Center for Molecular, Optical and Quantum Science and Department of Physics,
University of Oregon, Eugene, Oregon 97403, USA*

Temporal modes (TM) are a new basis for storage and retrieval of quantum information in states of light [1, 2]. The full TM manipulation toolkit requires a practical quantum pulse gate (QPG) [3, 4], which is a device that unitarily maps any given TM component of the optical input field onto a different, easily separable subspace or degree of freedom [5]. An ideal QPG must “separate” the selected TM component with unit efficiency, whilst avoiding crosstalk from orthogonal TMs [6]. All attempts at implementing QPGs in pulsed-pump traveling-wave systems have been unable to satisfy both conditions simultaneously [7–13]. This is due to a known selectivity limit in processes that rely on spatio-temporally local, nonlinear interactions between pulsed modes traveling at independent group velocities [6]. This limit is a consequence of time ordering in the quantum dynamical evolution [4, 14], which is predicted to be overcome by coherently cascading multiple stages of low-efficiency, but highly TM-discriminatory QPGs [15–17]. Multi-stage interferometric quantum frequency conversion in nonlinear waveguides was first proposed for precisely this purpose [15]. TM-nonspecific cascaded frequency conversion, also called optical Ramsey interferometry, has recently been demonstrated with continuous-wave (CW) fields [18, 19]. Here, we present the first experimental demonstration of TM-selective optical Ramsey interferometry and show a significant enhancement in TM selectivity over single-stage schemes.

All-optical quantum frequency conversion (QFC) by three- or four-wave mixing in nonlinear materials is well known to preserve the quantum state of light [20, 21]. These processes are in principle noiseless, and can be used at sub-unity conversion efficiencies (CE) to generate single-photon color-superposition states across disjoint frequency bands. This facet has been posited as a two-level Hilbert space for single-photon qubits [18]. Two QFC stages, each of which is set up for 50% CE, can be cascaded into a two-color interferometer constructed out of frequency-shifting beamsplitters. This effect has been shown for single-photon states in dual-pumped third-order nonlinear optical fibers [18], as well as for weak coherent states in singly-pumped second-order nonlinear waveguides [19]. Both of these instances utilized CW lasers for pumps, and very narrowband signals (single

photons, coherent states respectively) in their experiments.

Temporal modes are field-orthogonal broadband wavepacket states of light occupying a certain frequency band [22]. The CE of QFC devices can be made to be TM-selective, if the laser pump(s) have tailored pulse shapes [23]. To see this, we express the equations of motion for QFC in terms of temporal-mode envelope functions $A_j(z, t)$, where the index j labels the frequency band [6, 23]. For pulsed, three-wave mixing between pump (p -band), signal (s -band) and register (r -band) fields in a single-transverse-mode waveguide, the interaction Hamiltonian in a medium of length L is

$$\hat{H}_I(t) = \gamma \int_0^L dz A_p(t - \beta'_p z) \hat{A}_s(z, t) \hat{A}_r^\dagger(z, t) + h.a. \quad (1)$$

where we assume energy conservation ($\omega_r = \omega_p + \omega_s$) and phase-matching at the band central/carrier frequencies (ω_j). The parameters $\beta'_j \equiv \partial_\omega \beta(\omega)|_{\omega_j}$ are the group slownesses, or inverse-group velocities at said carrier frequencies. The temporal-mode envelope functions $\hat{A}_j(z, t)$ in the bands $j \in \{s, r\}$ have been elevated to photon creation operators $\{[\hat{A}_j(z, t), \hat{A}_{j'}^\dagger(z, t')] = \delta_{j,j'} \delta(t-t')\}$. Due to the linear nature of the field-evolution equations from the Hamiltonian in Eq. 1, the operators can also stand for the classical TM-functions of weak-coherent pulses [24]. The pump is assumed to be a strong, nondepleting coherent state, and its pulse-mode envelope is assumed square normalized ($\int_{-\infty}^{\infty} dt |A_p(t)|^2 = 1$). The coupling strength γ is proportional to the transverse-mode overlap integrals, the $\chi^{(2)}$ -nonlinear coefficient, as well as the square-root of the pump pulse energy.

Eq. 1 is identical in form to those governing a wide class of physical systems besides all-optical three-wave mixing. For instance, they can represent a pump-mediated interaction between an optical field and a collective Raman transition “spin-wave” in an atomic ensemble quantum memory [25, 26], implying that processes analogous to those studied here should also occur in such systems.

The phenomenon can be expressed as a scattering matrix relating input-mode operators $\hat{A}_j(z = 0, t')$ to output-mode operators $\hat{A}_j(z = L, t)$. It has been shown both theoretically and experimentally that for a wide range of system-parameter values ($\{\beta'_j, L, \gamma, \tau_p\}$, where τ_p is the pump pulse duration), at low effective-interaction

strengths ($\tilde{\gamma} = \gamma\sqrt{L/|\beta'_r - \beta'_s|}$), the frequency conversion is TM-discriminatory, with the target TM being dependent on the complex shape of the pump-pulse envelope [27]. But increasing the interaction strength to reach higher CE imposes a trade-off condition between target-TM CE and TM discrimination [6, 12]. This departure from high TM discrimination at large CEs is due to the effect of time-ordering corrections to the evolution [14]. The unitary evolution operator may be expressed in a Magnus expansion,

$$\hat{U}_I = \mathcal{T} \exp \left[-\frac{i}{\hbar} \int_{-\infty}^{\infty} dt \hat{H}_I(t) \right] = \exp(\hat{\Omega}_1 + \hat{\Omega}_2 + \hat{\Omega}_3 + \dots), \quad (2)$$

where \mathcal{T} imposes time ordering. The first-order perturbative term $\exp(\hat{\Omega}_1)$ is, by definition, sans time ordering effects. It has been shown in theory by us and others [15–17] that this limit to TM selectivity can be asymptotically overcome by preferentially weighing the first-order term in the expansion over the higher-order terms. This is achieved by coherently cascading multiple low-efficiency QFC stages in sequence. We have previously referred to this technique as temporal-mode interferometry (TMI). The basic schematic for a two-stage TMI is shown in fig. 1. The pump pulses for both stages are derived from a single pump beam to ensure constant relative phase. The net interferometric phase for the three-field process is $\Delta\Phi_p + \Delta\Phi_s - \Delta\Phi_r$.

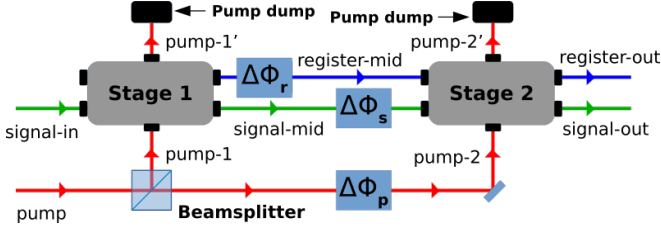


Figure 1. Schematic for a two-stage two-color optical Ramsey interferometer using three-wave mixing. If the medium dispersions are identical, then the pulse in the faster bands need to be delayed relative to those in the slower bands to ensure reinteraction in the second stage.

For this scheme to function, every stage needs to be highly TM-discriminatory, but not necessarily of high efficiency. The best parameter regime for high TM-discrimination at low CE is known to require that one of the weak bands (signal or register) copropagate with the pump pulse with a matching group velocity, and the other band’s group velocity be drastically different [4, 6]. In our system, this condition is approximately satisfied through the use of an MgO-doped PPLN waveguide quasi-phasematched for Type-0 second-harmonic generation from 816.6 nm to 408.3 nm. We center our pump and signal bands at 821 nm and 812.2 nm respectively, and chose their bandwidths such that the pump and signal pulse durations (~ 500 fs) are much larger than

the pump-signal inter-pulse walkoff within the length of the medium, thus effectively mimicking the group-velocity matching condition [11, 12].

The pump-signal walkoff scales linearly with medium length, implying that the group-velocity matching condition is better approximated in shorter waveguides. However, the single-stage TM-discrimination also requires that the register-band pulse walks off from the pump/signal pulse by a large amount [6]. This necessitates that the ratio of the effective interaction time and the pump duration $\zeta = (|\beta'_r - \beta'_s|L/\tau_p)$ be much larger than unity [12]. We work with a 5 mm long waveguide, yielding $\zeta \approx 10$, and a pump-signal walkoff of < 40 fs. Our pump and signal fields were derived from a home-built, Kerr-lens modelocked ultrafast Ti:sapphire laser producing pulses centered at 821 nm and with a FWHM spectral-intensity bandwidth of ~ 12 nm. The pulse repetition rate was 80 MHz. The laser pulses were then directed into a 4f pulse shaper detailed in the methods section.

The pump and signal-in pulses for the interferometer were generated by carving out their spectral components from the broadband ultrafast laser pulses in the pulse shaper [12]. We chose to work with modified Hermite-Gaussian functions with comparable bandwidths for the two-stage experiment. Specifically, we used three mode shapes defined as follows (with bandwidth parameter $\Delta\omega$, and normalization constants N_j):

$$HG0(\omega) = \frac{1}{\sqrt{N_0}} \exp\left(-\frac{(\omega - \omega_0)^2}{2\Delta\omega^2}\right), \quad (3)$$

$$HG1(\omega) = \frac{1}{\sqrt{N_1}} \left(\frac{\omega}{0.8\Delta\omega}\right) \exp\left(-\frac{(\omega - \omega_0)^2}{2(0.8\Delta\omega)^2}\right), \quad (4)$$

$$HG2(\omega) = \frac{1}{\sqrt{N_2}} \left[2\left(\frac{\omega}{0.89\Delta\omega}\right)^2 - 1 \right] \times \exp\left(-\frac{(\omega - \omega_0)^2}{2(0.8078\Delta\omega)^2}\right), \quad (5)$$

where ω is the angular frequency. The width modifications ensure mutual orthogonality whilst restricting total bandwidth of all three modes to the same neighborhood (~ 2.5 nm). Below, the pump and signal pulse shapes are denoted by pj and sj respectively, where index $j \in \{0, 1, 2\}$ refers to shape HGj from Eqs. 3-5. The pump and signal-in pulses are then sent towards the interferometer setup (see fig. 2).

The dispersion of the nonlinear media used in the two stages needs to be identical, to ensure phasematching between the same central wavelengths. We therefore reused the same waveguide twice, using a back-reflection-based doublepass “Michelson” scheme detailed in the figure. A broadband Faraday optical isolator enabled us to separate the “forward” and “backward” propagating pulses from the two stages, and measure the final outputs at its reject port. Longpass dichroic mirrors (labeled DM2

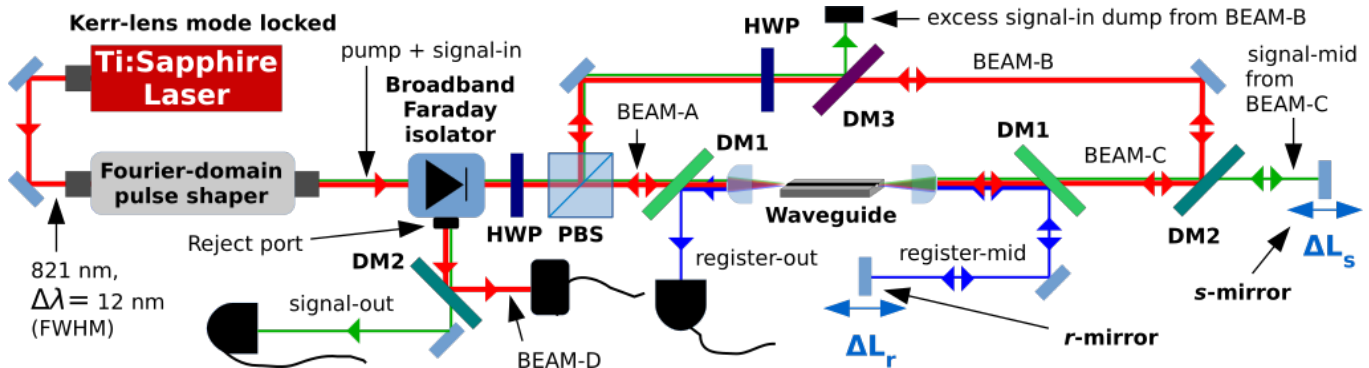


Figure 2. Two-stage, TM-selective optical Ramsey interferometer setup constructed by doublepassing all optical pulses through the same nonlinear MgO:PPLN waveguide. The pump pulse from the pulse shaper is split into two beams (A and B) at the polarizing beamsplitter (PBS). Pump-1 travels through the waveguide from left-to-right (beam-A to beam-C) and loops back to the PBS in the counterclockwise direction, and is eventually rejected into beam-D by the broadband Faraday isolator. Pump-2 travels along beam-B and goes through the waveguide from right-to-left (beam-C to beam-A), thus looping back to the PBS in the clockwise direction. The two pump pulses are within the waveguide at different times, forming the two stages. The signal-in pulse from beam-A copropagates with pump-1 through the waveguide, gets separated from the pump in beam-C through a dichroic mirror (DM2), and is then backreflected into the “second-stage” waveguide from an end mirror labeled “*s*-mirror.” The signal-out pulse from beam-A is measured at the reject port of the Faraday isolator. The register-mid pulse generated from partial conversion of signal-in in the first-stage is backreflected into the second stage from the “*r*-mirror.” All register-band pulses are separated/combined with the pump- and signal-band pulses using dichroic mirrors (DM1). The “*s*-mirror” and “*r*-mirror” elements are mounted on high-precision linear translation stages for effective interferometric phase control via subwavelength displacements ($\Delta L_j = \lambda_j \Delta \Phi_j / 2$ for $j \in \{s, r\}$). HWP stands for half-wave plate. DM3 is another dichroic element. Signal(register)-band beam paths are colored green(blue), while the pump-band beams are red.

in fig. 2) were used to split/combine the *r*-band pulses from the *s*- and *p*-band pulses. Similarly, other dichroic elements (DM1 and DM3 in fig. 2) were employed to split/combine the different bands in various permutations.

Both the signal-mid and register-mid pulses were backreflected off of flat mirrors mounted on high-precision linear translation stages. These mirrors, referred to as “*s*-mirror” (for signal) and “*r*-mirror” (for register), were used to ensure both proper pulse overlap in the second stage, as well as to impart interferometric phase via subwavelength displacements. For example, a fine displacement of ΔL_s in the signal-mid arm would impart a phase of $\Delta \Phi_s = 2\Delta L_s / \lambda_s$ to the interferometer, with the factor of two resulting from the doublepass path-length change.

All pulses were coupled into (and out of) the $5 \mu\text{m}$ wide PPLN waveguide using $f = 11 \text{ mm}$ aspheric lenses. The coupling efficiency into the waveguide was around 30%. Since the conversion efficiencies in the two stages need to match each other, to ensure sufficient pump energy in the second stage, we derived the pump-2 pulse afresh from the output of the shaper instead of backreflecting the transmitted pump-1 pulse. A half-wave plate and polarizing beamsplitter combination allowed us to independently redirect desired amounts of power into various beams. This freedom also enabled us to verify the identical operation of the waveguide in both directions by reproducing the single-stage results from [12] for both directions of propagation. A coupled average pump power

of 0.47 mW at a pulse rate of 80 MHz yielded a CE of 0.5 in both directions.

The fringe visibility of the two-stage interferometer is sensitive to any imbalance in effective losses between the signal and register arms. Kobayashi et al. [19] have modeled all the loss channels in the two-color interferometer as disjoint unitary beamsplitters placed at various beam locations in the setup. We matched the losses (due to absorption in various elements, as well as inefficient coupling into waveguide) between the signal-mid and register-mid beams by inserting a spatially varying ND filter into the beam path of the better coupled (signal-mid) arm.

Optical Ramsey-interference fringes were observed when recording the “internal” CE (defined as fraction of signal power depleted in the presence of pumps, which is independent of static losses) versus mirror displacements. Figure 3 plots the CE versus *s*-mirror displacement for various combinations of pump and signal TM shapes. The spatial peak-to-peak period was found to be roughly half the signal-band wavelength, consistent with the backreflection setup. Correspondingly, *r*-mirror displacements resulted in a spatial period of half the register-band wavelength (fig. 4(a)).

Figure 4(a) plots the CE fringe patterns for displacements of *r*-mirror alone (10 nm steps, legend item ‘A’), both *r*-mirror and *s*-mirror in opposite directions (10 nm and 20 nm steps respectively, legend item ‘B’), as well as both in the same direction (legend item ‘C’). Here, direc-

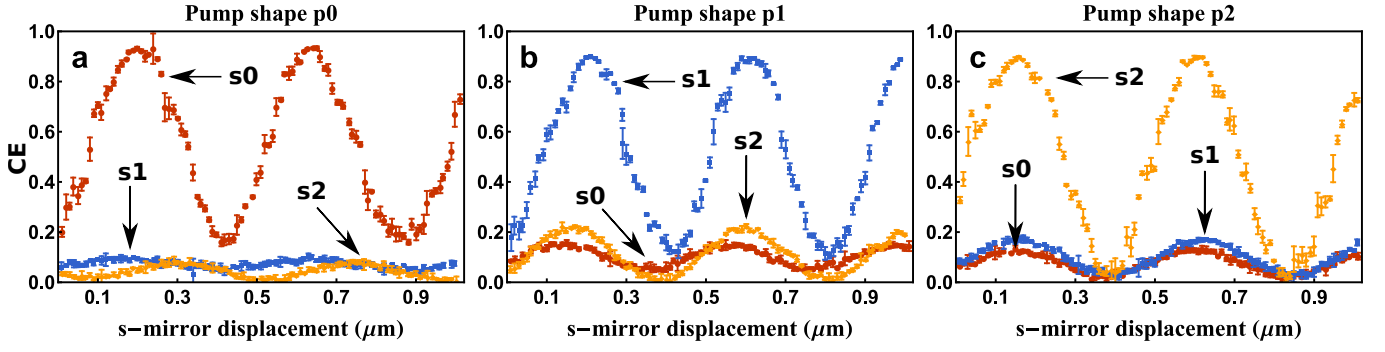


Figure 3. Two-stage, TM-selective optical Ramsey interferometric fringes visible in CE versus s -mirror displacement for pump-pulse shapes (a) p0, (b) p1, and (c) p2, with various signal TM shapes (s0, s1, s2). Shape functions defined in Eqs. 3-5. The relative phase shifts amongst the plots are due to system drifts in between data runs.

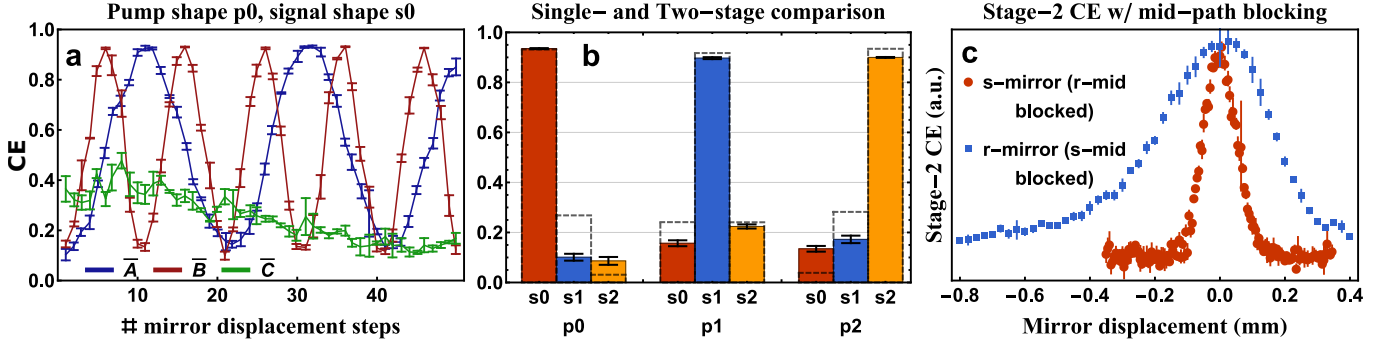


Figure 4. (a) Conversion efficiency versus combined-mirror-displacement for pump and signal shapes p0 and s0. r -mirror always moved in +10 nm steps. The legend items stand for s -mirror step sizes of 0 nm (A), -10 nm (B), and +10 nm (C). (b) Peak CE for various pump-signal shape combinations, and single-stage optimum levels for theoretically predicted exact Schmidt modes (dashed). (c) Cross correlation from Stage-2 only CE versus $s(r)$ -mirror displacement with register(signal)-mid beam blocked, demonstrating relative temporal widths. Pump and signal-in shapes were p0 and s0.

tion is “positive” towards the waveguide, i.e. shortening path length. Combined mirror displacements in opposite directions halved the fringe period, while the CE was nearly unchanging for matching directional moves, confirming the relative signs in the net interferometric phase formula ($\Delta\Phi_p + \Delta\Phi_s - \Delta\Phi_r$). Note that the register frequency is not an exact harmonic of the signal frequency.

The peak CE for the cases where the pump and signal TMs matched in shape far exceeded the shape-mismatched ones, as seen in fig. 4(b). Also plotted with dashed lines are the simulated single-stage CE for the theoretically predicted exact Schmidt modes at the pump powers required to match the maximum CE at each pump-pulse shape. The TM selectivity (roughly the contrast between targeted TM and other TMs) is enhanced for most shape combinations, even for signal TMs we used, which simply match the pump shapes (i.e. no attempt was made to optimize the signal pulses to match the exact Schmidt modes of the two-stage process). The single-stage results for the same waveguide and shaper slightly underperformed the numerical estimates [12].

The numerics assumed a parameter value $\zeta = (|\beta'_r - \beta'_s|L/\tau_p) = 10$. This must roughly equal the ratio of

the temporal width of the register-mid pulse to that of the pump/signal-in/signal-mid pulse [6]. We can estimate these widths by scanning the delay between pump-2 and the signal(register-mid) using $s(r)$ -mirror displacement and measuring the stage-2 CE while blocking the [register(signal)-mid] beam, as shown in fig. 4(c). The widths of pump-2 and signal-mid pulses will add in quadrature, since their group velocities are nearly equal. The pump-2 and idler-mid pulses, however, walk-off relative to each other in stage-2, resulting in a near-triangular CE curve. The data in fig. 4(c) indicates a $\zeta \sim 10$. It also demonstrates the expected temporal stretching of the register-mid pulse [6], related to the short SHG bandwidth of such waveguides [7, 8].

Stage-2 can separately be employed as a measurement device to demonstrate the effect of time ordering in the single-stage process. Figure 5 plots the stage-2 only CE versus s -mirror displacement for signal shapes s0 and s1 with the register-mid beam blocked. Both pump-1 and pump-2 are shaped p0, and the pump-2 beam is weak (averaging 0.1 mW at 80 MHz pulse rate). Figure 5(a) shows that the signal-mid pulse temporally skews to earlier times, as well as compresses in width relative to

signal-in pulse, as pump-1 power is increased. This illustrates the departure from the perturbative regime, and the distortion mimics the shape of the theoretically predicted single-stage output Schmidt modes [6]. The same is true for signal shape s1 (fig. 5(b)), as the second-Schmidt mode for a Gaussian pulse skews to later times [6].

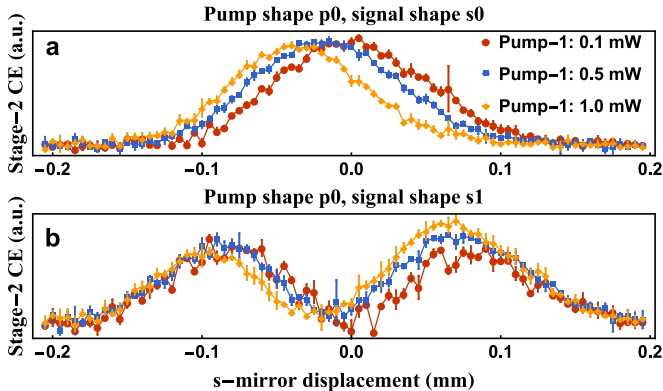


Figure 5. Stage-2 only CE versus s -mirror displacement with register-mid beam blocked for pump shape p0, and signal shape (a) s0, and (b) s1, at various pump-1 powers, and low pump-2 power. The average pump-1 beam powers listed in the legend are for pulse rates of 80 MHz. Positive displacement is towards the waveguide.

The direction of the temporal skewing in fig. 5(a) is consistent with the sign of the signal-register relative group slownesses ($\beta'_r - \beta'_s > 0$). The register amplitude generated inside the waveguide lags behind the copropagating pump-signal pulses, causing an enhanced depletion of the later half of the signal pulse. The skewing direction is not due to the small difference in the group velocities of the pump and signal bands. It would remain invariant under an exchange of labels between the p - and s -bands (and a corresponding exchange of powers/amplitudes, as the “pump”-band is defined as that which does not deplete).

The two-stage optical Ramsey interferometer was not only able to enhance TM selectivity over the single-stage variants (even for unoptimized, pump-shape-matched signal TMs), but was able to achieve large CE with a more efficient pump-photon budget. The results in fig. 3 and fig. 4(b) required beam powers of about 470 mW coupled in for both pump-1 and pump-2 (at 80 MHz pulse rates). Single-stage setups with the same waveguide could not reach such large CE for these net pump energies [12], even in theory [6, 17]. This is due to the double passage through the nonlinear medium. The gain in interaction strength due to extension of medium length is superior to that from increased pump power as the latter has a lower time-ordering penalty. The likeness of the exact Schmidt modes to the pump-pulse shape at low CE [3, 4, 6, 12, 15, 16] enabled us to demonstrate enhancement in TM selectivity without having to optimize the

signal-pulse shapes to match the said Schmidt modes.

In conclusion, we have demonstrated temporal-mode-selective quantum frequency conversion in a two-stage optical Ramsey interferometer by utilizing shape-tailored strong laser pump pulses and weak coherent signal pulses, and double passing through a single nonlinear optical waveguide in a Michelson configuration. We showed that there is a significant selectivity enhancement over single-stage implementations in agreement with theoretical predictions. We note that by changing the phase of one of the fields inside the Ramsey interferometer, our two-stage device also acts as a frequency-conversion switch that operates on one selected temporal mode and (approximately) not on the others. We verified the temporal distortion of the signal pulse during nonlinear interaction predicted by theory, and related that to time ordering effects in general multi-field interaction systems that are governed by similar dynamical equations. This technique provides fruitful insight into the nature of time-ordering in pulsed scattering processes and paves the way towards designing a fully selective quantum pulse gate, thus, opening up the temporal mode basis space for quantum information processing.

METHODS

Experimental setup details. The Fourier-domain, 4f pulse shaper used a 1800 lines/mm holographic grating in near-Littrow configuration, and a cylindrical lens of focal length 250 mm. We used a Meadowlark 8-bit, 2D, phase-only, reflective spatial light modulator of 1920×1152 pixel resolution and array size of 17.6 mm \times 10.7 mm in the Fourier plane of the pulse shaper. This allowed us to perform both amplitude and phase modulation using the Frumker-Silberberg first-order method [12, 28].

A Newport ISO-05-800-BB broadband Faraday optical isolator had a sufficiently flat transmission curve over a wide range of wavelengths for it to be deployed without imparting significant dispersion to the pump and signal-in pulses. The dichroic elements labeled DM1 in fig. 2 are the DMLP650 longpass dichroic mirrors from Thorlabs. The transmission edges of Semrock FF01-810/10 band-pass filters (DM2) and NF03-808E notch filters (DM3) were used to split/combine the p -band and s -band pulses from/with each other. The signal- and register- mirrors were mounted on Q-545.140 closed-loop servo linear stages from Physik Instruments, which had a nominal minimum step size of 6 nm, and an encoder-based position read-out precision of 1 nm. Low-profile flexure mounts from Siskiyou Inc. were used inbetween the two stages to construct a stable interferometer. Servo motors controlled by microcontrollers were used as beam blocks at various locations for convenience.

* dileep@uoregon.edu

- [1] J. P. Heritage and A. M. Weiner, *IEEE J. Sel. Top. Quantum Electron.* **13**, 1351 (2007).
- [2] B. Brecht, D. V. Reddy, C. Silberhorn, and M. G. Raymer, *Phys. Rev. X* **5**, 041017 (2015).
- [3] A. Eckstein, B. Brecht, and C. Silberhorn, *Opt. Express* **19**, 13770 (2011).
- [4] B. Brecht, A. Eckstein, A. Christ, H. Suche, and C. Silberhorn, *New J. Phys.* **13**, 065029 (2011).
- [5] Y.-P. Huang and P. Kumar, *Opt. Lett.* **38**, 468 (2013).
- [6] D. V. Reddy, M. G. Raymer, C. J. McKinstrie, L. Mejling, and K. Rottwitt, *Opt. Express* **21**, 13840 (2013).
- [7] Z. Zheng and A. M. Weiner, *Chemical Physics* **267**, 161 (2001).
- [8] Z. Zheng, A. M. Weiner, K. R. Parameswaran, M.-H. Chou, and M. M. Fejer, *J. Opt. Soc. Am. B* **19**, 839 (2002).
- [9] B. Brecht, A. Eckstein, R. Ricken, V. Quiring, H. Suche, L. Sansoni, and C. Silberhorn, *Phys. Rev. A* **90**, 030302 (2014).
- [10] V. Ansari, M. Allgaier, L. Sasoni, B. Brecht, J. Roslund, N. Treps, G. Harder, and C. Silberhorn, *arXiv:1607.03001v1* (2016), *arXiv:1607.03001v1 [quant-ph]*.
- [11] P. Manurkar, N. Jain, M. Silver, Y.-P. Huang, C. Langrock, M. M. Fejer, P. Kumar, and G. S. Kanter, *Optica* **3**, 1300 (2016).
- [12] D. V. Reddy and M. G. Raymer, *Opt. Express* **25**, 12952 (2017).
- [13] A. Shahverdi, Y. M. Sua, L. Tumeh, and Y.-P. Huang, *Sci. Rep.* **7**, 2045 (2017).
- [14] N. Quesada and J. E. Sipe, *Phys. Rev. A* **90**, 063840 (2014).
- [15] D. V. Reddy, M. G. Raymer, and C. J. McKinstrie, *Optics Letters* **39**, 2924 (2014).
- [16] D. V. Reddy, M. G. Raymer, and C. J. McKinstrie, *Phys. Rev. A* **91**, 012323 (2015).
- [17] N. Quesada and J. E. Sipe, *Opt. Lett.* **41**, 364 (2016).
- [18] S. Clemmen, A. Farsi, S. Ramelow, and A. L. Gaeta, *Phys. Rev. Lett.* **117**, 223601 (2016).
- [19] T. Kobayashi, D. Yamazaki, K. Matsuki, R. Ikuta, S. Miki, T. Yamashita, H. Terai, T. Yamamoto, M. Koashi, and N. Imoto, *Opt. Express* **25**, 12052 (2017).
- [20] J. Huang and P. Kumar, *Phys. Rev. Lett.* **68**, 2153 (1992).
- [21] H. J. McGuinness, M. G. Raymer, C. J. McKinstrie, and S. Radic, *Phys. Rev. Lett.* **105**, 093604 (2010).
- [22] U. M. Titulaer and R. J. Glauber, *Phys. Rev.* **145**, 1041 (1966).
- [23] C. J. McKinstrie, L. Mejling, M. G. Raymer, and K. Rottwitt, *Phys. Rev. A* **85**, 053829 (2012).
- [24] U. M. Titulaer and R. J. Glauber, *Phys. Rev.* **145**, 1041 (1966).
- [25] J. I. Cirac, L. M. Duan, and P. Zöller, *arXiv:quant-ph/0405030* (2004), *arXiv:quant-ph/0405030 [quant-ph]*.
- [26] J. Nunn, I. A. Walmsley, M. G. Raymer, K. Surmacz, F. C. Waldermann, Z. Wang, and D. Jaksch, *Phys. Rev. A* **75**, 011401 (2007).
- [27] L. Mejling, D. S. Cargill, C. J. McKinstrie, K. Rottwitt, and R. O. Moore, *Opt. Express* **20**, 27454 (2012).
- [28] E. Frumker and Y. Silberberg, *J. Opt. Soc. Am. B* **24**, 2940 (2007).

ACKNOWLEDGEMENTS

This work was supported by a grant from the National Science Foundation (NSF)(1521466), QIS - Quantum Information Science Program. We owe much to the theoretical analysis of Dr. Colin McKinstrie. We also thank Prof. Steven van Enk and Prof. Brian J. Smith for discussions and suggestions regarding the experiment. We thank Phil Battle and David Walsh AdvR for providing us with the waveguide.

AUTHOR CONTRIBUTIONS

DVR conceived of the idea in the context of TM selectivity, and design and built the whole setup. DVR also collected and analyzed the data. MGR supervised the project closely. DVR prepared the manuscript, with inputs from MGR.